

# Frequency decoding subject to dose conservation: firing rate response of periodically driven spiking models\*

A. Granados      M. Krupa      F. Clément

## Abstract

In this work we consider a periodically forced generic integrate-and-fire model with a unique attracting equilibrium in the subthreshold dynamics and study the dependence of the firing rate on the frequency of the drive. The biological motivation underlying this work is the differential control exerted by the hypothalamic gonadotropin releasing hormone (GnRH), which is secreted in a pulsatile manner, on the secretion of the pituitary hormones FSH (follicle stimulating hormone) and LH (lutening hormone) according to GnRH pulse frequency. Our forcing satisfies the constraint of dose conservation, which can be interpreted as fixing the average GnRH concentration, while the frequency, amplitude and duty cycle are allowed to vary. The bifurcation structure in the parameter space formed by these last ones has been rigorously studied in [GKC13] where the firing rate was related with the rotation number of the existing periodic orbits. In this work we rigorously study how these bifurcation structures behave upon frequency variation. This allows us to show that the dependence of the firing rate on frequency of the drive follows a devil's staircase with non-monotonic steps and that there is an optimal response in the whole frequency domain. We also characterize certain bounded frequency windows in which the firing rate exhibits a bell-shaped envelope with a global maximum.

## 1 Introduction

In this work we study periodically driven excitable systems of integrate and fire type, widely used to model excitable cells. We assume that the periodic forcing term, or the external input, satisfies a constraint which we refer to as dose conservation. The constraint is defined as fixing the total amount (cumulated dose) in a given time (observation time). As argued in §2.1, this is equivalent to fixing the average rate of the cell stimulus, for example the applied current,

---

\*This work has been financially supported by the Large Scale Initiative Action REGATE, by the Spanish MINECO-FEDER Grants MTM2009-06973, MTM2012-31714 and the Catalan Grant 2009SGR859

the amount of neurotransmitter, or the amount of hormone per time unit, respectively. One of the goals of this work is to prove that the system exhibits an optimal response, in terms of the firing rate, which can be achieved by tuning the system parameters, like period or amplitude, to obtain the maximal firing rate of the system (the average number of spikes per unit time). In particular, we consider square wave input and focus on the variation of the period while either the amplitude or the duration of the pulse is fixed.

The mathematical content of our study is to investigate the bifurcation structure of periodic orbits, as they completely determine the dynamics for the class of systems we study. In contrast to other studies [KHR81, CB99, CO00, Coo01, COS01, CTW12, TB08, TB09, LC05], which use Poincaré maps, our approach is by means of a stroboscopic map. This map is discontinuous, but it has the advantage of being contracting on the continuous components. Hence, as shown in [GKC13], results in non-smooth systems can be applied to get a complete description of periodic orbits and their rotation numbers. In this work we use this information to understand firing rates. In particular, it we prove the existence of an optimal response corresponding to the maximal firing rate.

Frequency encoding of signals is a common occurrence in biological systems. One of the most ubiquitous instances is intracellular calcium signaling through Calcium spikes, that has been subject of numerous studies (see e.g. [TBH<sup>+</sup>96]). However, most of the time, the impact of changes in the frequency cannot be distinguished from that of the other signal properties, especially the cumulated dose, which blurs the intrinsic effect of frequency. In the field of neuroendocrinology, the hypothalamo-hypophyso-gonadal (HHG) axis offers a typical instance of “genuine frequency effect”, that is the main motivation of this paper: the differential control exerted by the hypothalamic gonadotropin releasing hormone (GnRH) on the secretion of the pituitary hormones FSH (follicle stimulating hormone) and LH (luteinizing hormone) according to GnRH pulse frequency.

The setting we have chosen for this paper is very simple from the biological point of view, but it has the advantage of being mathematically tractable. This is mainly given by assuming that the unforced system possesses a unique attracting point in the subthreshold dynamics. Even simple generalizations, for example allowing the system to undergo a subthreshold saddle-node bifurcation, lead to complications, as the stroboscopic map can have expanding pieces, so that the existence of a globally stable attractor cannot be expected. In particular it is not clear if the firing rate can be uniquely defined in the context of such generalizations, as well as how to obtain rigorous results about it.

The main result of this paper is a complete description of the response of the system, in terms of the firing rate, to frequency variation. In particular, we prove that the firing rate is maximal for a certain frequency which depends on the features of the stimulus (amplitude and duty cycle) as well as on the dynamical properties of the system. In addition, we provide detailed information on how to compute such frequency and the corresponding maximal value of the firing rate.

This work is organized as follows.

In §2.2 we describe the integrate-and-fire system, provide some definitions and state our results. In §3.1 we describe a bifurcation scenario established in our earlier work [GKC13], which we use to prove our results. In §3.2 we describe how the bifurcations in this parameter space change under frequency variation. We also provide a precise statement of our results and their proofs. In §3.3 we present a result regarding the optimization of the firing rate in terms of frequency of the input. Finally, in §4 we apply these results to an example, a linear integrate-and-fire neuron (LIF), to completely describe the firing rate response under frequency variation.

## 2 The model

### 2.1 Motivation

GnRH is the master hormone controlling the reproductive axis. It is released by dedicated hypothalamic neurons in a pulsatile manner and reaches its target pituitary cells through a specific portal system that preserves the dynamical properties of the GnRH signal.

The modulation of GnRH pulse frequency is observed in natural situations along the ovarian cycle and can be experimentally mimicked in castrated males exposed to different regimes of GnRH pulses (see [BNXR10] for a review on GnRH signaling). This frequency modulation is responsible for the differential control of FSH and LH, although both hormones are secreted by the same type of pituitary cells, the gonadotrophs. The frequency-dependent response can notably be observed at the level of gene expression, with a non-monotonic expression of the common  $\alpha$  subunit and FSH or LH-specific  $\beta$  subunit according to the frequency; there appears to exist an optimal frequency of stimulation that differs amongst the FSH $\beta$  and LH $\beta$  subunit.

On the experimental ground, several authors have checked the “genuine” frequency dependence of the response by controlling the total dose of GnRH administered along the experiments, either *in vitro* (in primary monolayer cultures of rat pituitary cells) [KJSC97] or *in vivo* (from “fresh” pituitaries removed from castrated male rats) [DHO<sup>+</sup>89]. On the physiological ground, there is also evidence that changes in frequency are not accompanied with increased cumulated dose [EDGK97].

In this paper, we investigate the question of GnRH frequency decoding from a purely dynamical viewpoint. We do not account at all for the biochemical pathways involved in GnRH signaling in pituitary cells, but rather consider a compact input-output function aggregating the whole sequence from the upstream event of GnRH binding to its receptor up to the downstream response of pituitary cells in term of expression rates of the different gonadotropin subunits. More precisely, we choose a generic integrate-and-fire type model exhibiting sub-

threshold attracting dynamics, as an approximation of spiking dynamics for excitable cells. In such an approximation, the response exhibited by the excitable system in the form of a large amplitude oscillation (spike) is replaced in the integrate-and-fire model by a discontinuity of the trajectory, which occurs when the system reaches a certain previously designed threshold. Our goal is then to study the response of the system upon frequency variation of the stimulating square wave function. This reaction will be measured in terms of the so called firing rate.

The GnRH pulse can be roughly considered as square-wave shaped [MK92]: pulsatile events of secretion are separated by time intervals when the GnRH level goes back to the baseline (where signal is almost off). Even though there exist models of the GnRH pulse generator, that were previously developed in the setting of slow-fast dynamics [CF07], we will not use the output of such models to generate our input signal  $I(t)$ , but directly simulate a “strict” square-wave signal, which allows us to control directly the period, duration and amplitude of the input.

A recent work [MHR12] considers a rectified sinusoidal to study properties of the firing rate in the context of type III excitability (variable threshold).

Regarding the cumulative dose constraint, we first assume that the observation time,  $\tau$ , is large enough relative to the different periods of the signal,  $T$ . Hence, the total amount of released quantity can be approximated by

$$\int_0^\tau I(t)dt \sim Q\tau,$$

where  $Q$  is the average value of  $I$  over one period,

$$Q := \frac{1}{T} \int_0^T I(t)dt,$$

which we will call *dose*. Hence, as long as the previous assumption is satisfied, the cumulative dose will be maintained as long as the dose  $Q$  is conserved. We will refer to this as *dose conservation*.

The square wave function  $I(t)$  will be characterized by three parameters: its amplitude  $A$ , its period  $T$  and the *duty cycle*  $d$ , which is the duration of the pulse with respect to  $T$ .

In order to apply the dose conservation, one has only to keep constant the product  $Ad$ , which can be performed in different ways. In this work we will focus on two of them, the trivial one by keeping constant both  $A$  and  $d$  (width correction) and also the other one varying both  $A$  and  $d$  so that the total duration of the pulse,  $\Delta = dT$ , is constant (amplitude correction).

We will obtain theoretical results for the first case, which will be used also to study the behavior of the firing rate under frequency variation for the second case in an example in §4.3.

## 2.2 Definitions and statement of results

We consider a non-autonomous periodic system given by

$$\dot{x} = f(x) + I(t), \quad x \in \mathbb{R} \quad (2.1)$$

with  $f(x) \in C^\infty(\mathbb{R})$  and  $I(t)$  a  $T$ -periodic square-wave function

$$I(t) = \begin{cases} A & \text{if } t \in (nT, nT + dT] \\ 0 & \text{if } t \in (nT + dT, (n+1)T], \end{cases} \quad (2.2)$$

with  $0 \leq d \leq 1$ . We submit system (2.1) to the reset condition

$$x = \theta \longrightarrow x = 0, \quad (2.3)$$

that is, the trajectories of system (2.1) are instantaneously reset to 0 whenever they reach the threshold given by  $x = \theta$ . This provides a new system which is typically considered to be in the class of *hybrid* systems, due to the combination of an algebraic condition and a differential equation. Due to the generality of the function  $f$ , this system represents a large class of the so-called *integrate-and-fire* models which are best known for their use as simplification of excitable systems modeling neurons. Hence, we will refer to the discontinuities given by the reset condition as spikes, as they emulate the typical spiking oscillations performed by such systems in response to some input.

Despite these discontinuities, the solutions of the non-autonomous system (2.1)-(2.3) are well defined. Let  $\phi(t; t_0, x_0)$  be the solution of system (2.1)-(2.3) fulfilling  $\phi(t_0; t_0, x_0) = x_0$ . As usual in piecewise-smooth systems, the flow  $\phi$  is obtained by properly matching the solutions for  $0 < t \bmod T \leq dT$  and  $dT < t \bmod T \leq T - dT$  combined with the reset condition (2.3). This makes the flow  $\phi$  non-differentiable at  $t \bmod T = dT$  and  $t \bmod T = T$  and discontinuous at the spikes times, those at which the threshold is reached.

**Remark 2.1.** *As we are interested in periodic orbits, although system (2.1)-(2.3) is non-autonomous, we will assume from now on that  $t_0 = 0$ , and we will write  $\phi(t; x_0)$ . Note that if  $t_0 \neq 0$ , the initial condition for a periodic orbit (fixed point of the stroboscopic map) may be different, although it still exists.*

Let us assume that the system

$$\dot{x} = f(x) \quad (2.4)$$

satisfies the following conditions.

H.1 (2.4) possesses an attracting equilibrium point

$$0 < \bar{x} < \theta, \quad (2.5)$$

H.2  $f(x)$  is monotonic decreasing function in  $[0, \theta]$ :

$$f'(x) < 0, \quad 0 \leq x \leq \theta.$$

As shown in [GKC13], system (2.1)-(2.3) possesses attracting periodic orbits for almost all (except in a cantor set with zero measure) values of  $T$ ,  $A$ ,  $\theta$  and  $d$  as long as conditions H.1-H.2 are satisfied. These periodic orbits may be continuous (subthreshold dynamics) or discontinuous (spiking dynamics). Let  $\phi(t; x_0)$ , with  $\phi(0; x_0) = x_0$ , be an orbit of the non-autonomous system (2.1)-(2.3). Then we consider

$$r(x_0) = \lim_{\tau \rightarrow \infty} \frac{\#(\text{spikes performed by } \phi(t; x_0) \text{ for } t \in [0, \tau])}{\tau}, \quad (2.6)$$

where  $\#$  means *number of*, if this limit exists. We then define the *firing rate*.

**Definition 2.1.** *If  $r(x_0)$  does not depend on  $x_0$  then we call it  $r$ , the firing rate.*

The firing rate can be seen as the average number of spikes per unit time performed by the system along a periodic orbit.

Note that the firing rate is well defined whenever there exists a unique attracting periodic orbit. However, it will in general depend on the system parameters  $T$ ,  $A$  and  $d$ .

Unlike in other approaches ([KHR81, CB99, CO00, COS01, CTW12, TB08]), in order to study integrate-and-fire model (2.1)-(2.3) our essential tool will be the stroboscopic map. Given an initial condition  $x_0$ , this map consists in flowing the system (2.1)-(2.3) for a time  $T$ , the period of the perturbation, and is the usual tool used when dealing with (smooth) periodic non-autonomous systems. In other words, it becomes

$$\mathfrak{s}(x_0) = \phi(T; x_0), \quad (2.7)$$

where  $\phi(t; x_0)$  is the flow associated with (2.1)-(2.3). In the mentioned works, authors considered a Poincaré map from the threshold to itself (when spikes occur), added time as a variable and studied the times given by the spikes.

The discontinuities exhibited by  $\phi(t; x_0)$  at the spiking times will make the map  $\mathfrak{s}(x_0)$  be piecewise-defined and discontinuous, and hence it is typically avoided in such type of systems, as one cannot apply classical results for regular smooth systems. However, using results in non-smooth systems, the dynamics of the map is completely understood (see [GKC13] for a discussion and references). This includes the rotation number, also called winding number,  $\rho$ , of all possible periodic orbits of the stroboscopic map, which will be of special interest in our work. The rotation number is usually associated with circle maps and, intuitively, measures the average rotation along trajectories when it does not depend on its initial condition. Under certain conditions, discontinuous piecewise-defined maps can be reduced to circle maps, and, when a periodic orbit exists, the rotation number becomes the ratio between the number of steps at the right of the discontinuity along the periodic orbits to its period.

As shown in [KHR81] (see also [GKC13] and section §3.1 below), the rotation number of the periodic orbits is well related with the number of spikes performed at each period of a periodic orbit of the stroboscopic map. A crucial quantity will be the average number of spikes by period of the stroboscopic map, which

was named in [KHR81] *firing-number*,  $\eta$ . This is given more precisely by the following definition.

**Definition 2.2.** *Let  $n$  be the total number of spikes performed by a  $p$ -periodic orbit of the stroboscopic map  $\mathfrak{s}(x)$ ,  $n, p \in \mathbb{N}$ ; then we define the firing-number as*

$$\eta = \frac{n}{p}, \quad (2.8)$$

*which is the average number of spikes per iteration of the stroboscopic map along a periodic orbit.*

**Remark 2.2.** *Then, assuming that the mentioned periodic orbit is attracting, the firing rate can be obtained from the firing-number as*

$$r = \frac{\eta}{T}. \quad (2.9)$$

As mentioned in §2.1, one of the quantities that will play an important role in our results is the average of the input  $I(t)$ ,

$$\frac{1}{T} \int_0^T I(t) dt = Ad := Q, \quad (2.10)$$

which we will refer as *dose*.

As shown below, depending on the value of  $Q$  the firing rate will exhibit qualitatively different behaviors. This will bring us to consider a *critical dose*, which we define as follows.

**Definition 2.3.** *The critical dose,  $Q_c$ , is the value of  $A > 0$  that places the equilibrium point,  $\bar{x}$ , of the system  $\dot{x} = f(x) + A$  at the threshold; it is given by*

$$f(\theta) + Q_c = 0. \quad (2.11)$$

Note that  $Q_c$  is the minimal dose that permits the system (2.1)-(2.3) to exhibit spikes when it is driven constantly,  $I(t) = Q_c$  ( $d = 1$  and  $A = Q_c$ ).

Our goal is to study the qualitative behavior of the firing rate under variation of the period of the input,  $T$ , for a chosen  $Q$ . We then prove the following results when  $A > 0$  and  $d \in (0, 1)$  are kept constant (with correction for dose conservation).

1. The firing rate, obtained as the ratio of the firing-number  $\eta$  to  $T$ , follows a devil's staircase with monotonically decreasing steps (see figure 2.1). This is a consequence of propositions 3.1 and 3.2 (corollary 3.2).
2. The firing rate for low frequency inputs fulfills

$$\lim_{T \rightarrow \infty} r(T) = \frac{d}{\delta},$$

where  $\delta$  is the time needed by system  $\dot{x} = f(x) + A$  to reach the threshold from  $x = 0$ . This is proposition 3.3.

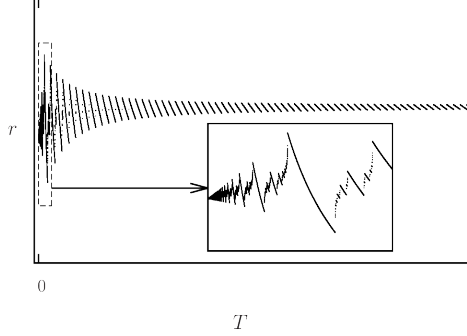


Figure 2.1: Typical response of the firing rate upon frequency variation. It is given by a fractal structure of monotonically decreasing pieces, following a devil’s staircase. The width of the “main pieces” stabilizes at  $O(\delta/d)$ , and each exhibits a local maximum and minimum. The firing rate has limiting value  $d/\delta$  when  $T \rightarrow \infty$ , and  $1/\hat{\delta}$  when  $T \rightarrow 0$ , and it exhibits a global maximum and minimum.

3. If  $I(t)$  is such that  $Q = Ad < Q_c$ , then the firing rate becomes zero for large enough frequencies. This is also a consequence of propositions 3.1 and 3.2 (corollary 3.1).

4. If  $Q > Q_c$ , then

$$\lim_{T \rightarrow 0} r(T) = \frac{1}{\hat{\delta}},$$

where  $\hat{\delta} > 0$  is the time needed for the averaged system  $\dot{x} = f(x) + Ad$  to reach the threshold from  $x = 0$ . This is proposition 3.4.

5. The firing rate exhibits a global maximum and minimum in  $T \in (0, \infty)$ . Let  $0 < T_1 < T_2$  such that  $\eta(T) = 1$  for  $T \in (T_1, T_2)$ . Then, if  $T_1$  is large enough, the maximal firing rate occurs for  $T = T_1$ . The minimal one corresponds to the minimum between  $0, 1/\hat{\delta}$  (see 4.) and  $1/T_2$ . This is proposition 3.5 and remark 3.10.

### 3 Bifurcation analysis

#### 3.1 The two-dimensional parameter space

In this section we provide a summary of the results shown in [GKC13], see there for the details and proofs of what follows in this section.

As mentioned in §2.2, due to the periodicity of  $I(t)$ , we will use the stroboscopic map (2.7), which is a discontinuous piecewise-smooth map, in order to



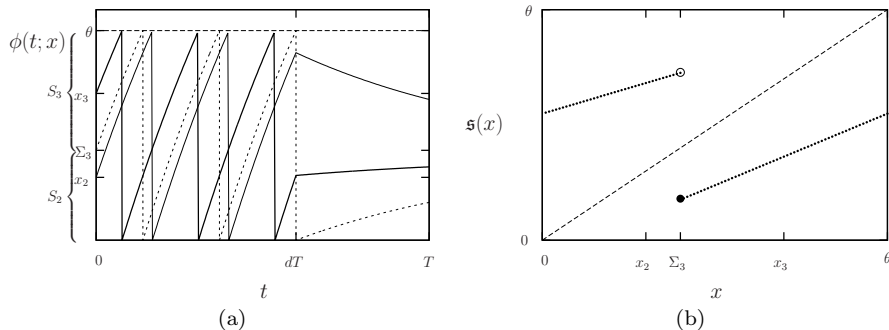


Figure 3.1: In (a) the trajectories of systems (2.1)-(2.3). Dashed line: trajectory with  $\Sigma_3$  as initial condition. Thick line: trajectory with  $x_3 > \Sigma_3$  as initial condition, which spikes 3 times. Normal line: trajectory with  $x_2 < \Sigma_3$  as initial condition, which spikes 2 times. In (b) the stroboscopic map, with a discontinuity at  $x = \Sigma_3$ .

understand the dynamics of system (2.1)-(2.3). This map is a smooth map (as regular as  $f(x)$  (2.1)) in certain regions in the state space  $[0, \theta]$  characterized by the number of spikes performed by  $\phi$ , the discontinuous flow associated with system (2.1)-(2.3), when flowed for a time  $T$ . This is because, in these regions, the stroboscopic map becomes a composition of maps obtained by integrating system (2.1) and resetting from  $x = \theta$  to  $x = 0$ . Both types of intermediate maps are smooth. These regions in the state space are separated by boundaries of the form  $x = \Sigma_n$ ,  $\Sigma_n = \Sigma_n(A, T, d)$ , where the stroboscopic map is discontinuous. At the right of  $x = \Sigma_n$  the trajectories of (2.1)-(2.3) exhibit  $n$  spikes when flowed for a time  $T$ , whereas at its left they exhibit  $n - 1$  spikes (see figure 3.1 for  $n = 3$ ).

As the number of spikes can be arbitrarily large (for  $A > 0$  large enough), the state space  $[0, \theta]$  is potentially divided in an infinite number of such regions. However, for fixed parameter values, the state space is split in at most two regions,  $[0, \Sigma_n)$  and  $[\Sigma_n, \theta)$ , where the trajectories perform  $n - 1$  and  $n$  spikes, respectively, when flowed during a time  $T$ .

The possible dynamics of the stroboscopic map, and hence of system (2.1)-(2.3), is completely captured in the two-dimensional parameter space  $d \times 1/A$ . Thus, by understanding the bifurcation structures in this parameter space one obtains a complete description of the fixed points, periodic orbits, their rotation numbers and their firing rate.

Under the assumptions H.1-H.2, the bifurcation scenario in the parameter space given by  $d \times 1/A$  for  $T > 0$  is equivalent to the one shown in figure 3.2.

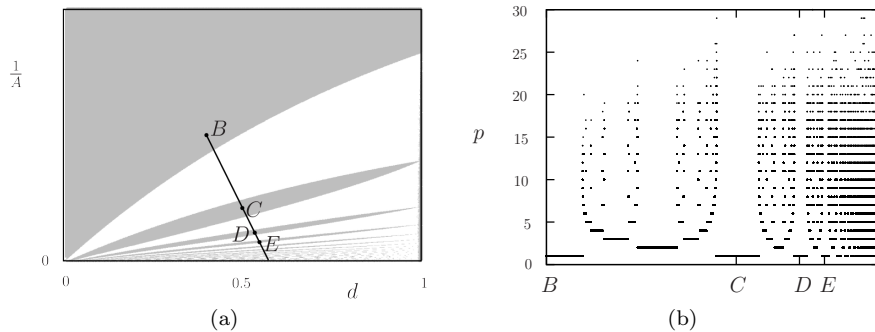


Figure 3.2: (a) Bifurcation scenario for system (2.1)-(2.3). In gray regions there exist  $T$ -periodic orbits, in white ones higher periodic orbits following and adding structure (see text). In  $B$ ,  $C$ ,  $D$  and  $E$  one finds  $T$ -periodic orbits spiking 0, 1, 2 and 3 times per period, respectively. (b) Periods of the periodic orbits found along the segment shown in (a).

As suggested in figure 2(a), there exists an infinite number of regions (in gray) accumulating to the horizontal axis for which only  $T$ -periodic orbits spiking  $n$  times exist. These are fixed points,  $\bar{x}_n$ , of the stroboscopic map  $\mathfrak{s}(x)$  (2.7). These regions in parameter space are ordered, in the clockwise direction, in such a way that these  $T$ -periodic orbits spike 0, 1, 2, 3,  $\dots$  times per period. The bifurcation curves that bound the gray regions are given by border collision bifurcation of the map. That is, the fixed points of the stroboscopic map  $\bar{x}_n$  collide with one of the boundaries,  $\bar{x}_n = \Sigma_n$  (figures 3(a) and 4(a) for  $n = 3$ ) and  $\bar{x}_n = \Sigma_{n+1}$  (figures 3(d) and 4(d) for  $n = 3$ ), and no longer exist. This defines the upper and lower bifurcation curves, respectively, bounding each gray region as follows.

**Definition 3.1.** For  $d \in (0, 1)$ , we define  $A_n^{\mathcal{R}}(d)$  and  $A_n^{\mathcal{L}}(d)$ ,  $n \geq 1$ , the values of  $A$  for which the fixed point  $\bar{x}_n$  collides with the boundaries  $\Sigma_n$  and  $\Sigma_{n+1}$ , respectively:

$$\lim_{A \rightarrow (A_n^{\mathcal{R}})^+} \bar{x}_n = \Sigma_n$$

$$\lim_{A \rightarrow (A_n^{\mathcal{L}})^-} \bar{x}_n = \Sigma_{n+1}.$$

The fixed point  $\bar{x}_0 \in S_0$  undergoes only one border collision bifurcation, when it collides with  $\Sigma_1$  from the left. This one occurs for  $A = A_0(d)$ ,

$$\lim_{A \rightarrow (A_0)^-} \bar{x}_0 = \Sigma_1.$$

Hence, a fixed point  $\bar{x}_n \in S_n$  will exist if  $A \in [A_n^{\mathcal{R}}, A_n^{\mathcal{L}})$ .

**Remark 3.1.** *The values  $A_n^{\mathcal{R}, \mathcal{L}}(d)$  depend also on  $T$ ; we will explicitly specify this when convenient.*

At the upper bifurcation curves ( $A = A_n^{\mathcal{R}}(d)$ ), the fixed points collide with a boundary from its right (figures 3(a) and 4(a)), and hence will be associated to the  $\mathcal{R}$  symbol. On the lower ones ( $A = A_n^{\mathcal{L}}(d)$ ) fixed points collide with another boundary from its left (see figures 3(d) and 4(d)), and will have associated the symbol  $\mathcal{L}$ . Note that the stroboscopic map fulfills  $\mathfrak{s}(\Sigma_n) = \mathfrak{s}(\Sigma_n^+)$ , and hence the fixed points no longer exist at their left bifurcations whereas they still do for the right bifurcations (note the gray shown in figures 3(d) and 4(d)). The first bifurcation defining the uppermost bifurcation curve, given by  $\bar{x}_0 = \Sigma_1$  ( $A = A_0(d)$ ), is a bit different than the others, as it separates the parameter space  $d \times 1/A$  in two regions. In the lower side of the bifurcation curve, only spiking asymptotic dynamics are possible whereas on the upper side only a continuous  $T$ -periodic orbit exhibiting no spike can exist.

When entering the white regions, the map does no longer possess any fixed point. Instead, periodic orbits with arbitrarily high periods exist. These are shown in figure 2(b) along the segment shown in figure 2(a). As can be observed, they are organized by the period adding structure; that is, between two periodic orbits with periods  $p$  and  $q$ , there exists another periodic orbit with period  $p+q$ .

As usual in piecewise-smooth dynamics, one can encode periodic orbits by introducing symbolic dynamics as follows. We assign the letters  $\mathcal{L}$  and  $\mathcal{R}$  depending on whether the corresponding periodic orbit steps on the left or on the right of the discontinuity. Then, the adding phenomenon is given by the concatenation of symbolic sequences; that is, between two regions in parameter space where the periodic orbits with symbolic sequences  $\sigma$  and  $\omega$  exist, there exists a region locating a periodic orbit with symbolic sequence  $\sigma\omega$ , whose period is the addition of the two previous ones. In figure 3.5 we show the symbolic sequences of the periodic orbits found along the line shown in figure 2(a) when crossing the white region between points  $B$  and  $C$ , as well as their associated rotation numbers. These numbers are obtained by dividing the number of  $\mathcal{R}$ 's contained in the symbolic sequence by its total length (the period of the periodic orbit).

Note that the rotation numbers are organized by the so-called Farey tree associated with the period-adding phenomenon. Other authors [FG11] suggest that this should be given by a Stern-Brocot tree. However, it is the Farey tree that needs to be considered in the context of the period adding, as it contains more precise information in the form of rotation numbers (see for example [GGT84, GIT84]). As a consequence, the rotation number follows a devil's staircase from 0 to 1. This is a monotonically increasing function which is constant almost everywhere, except in a Cantor set of zero measure.

Immediately after crossing a white region and entering a gray one where another  $T$ -periodic orbit exists (fixed point of the stroboscopic map), the rotation number equals 1 for a while until it suddenly jumps to 0 again. This is due to

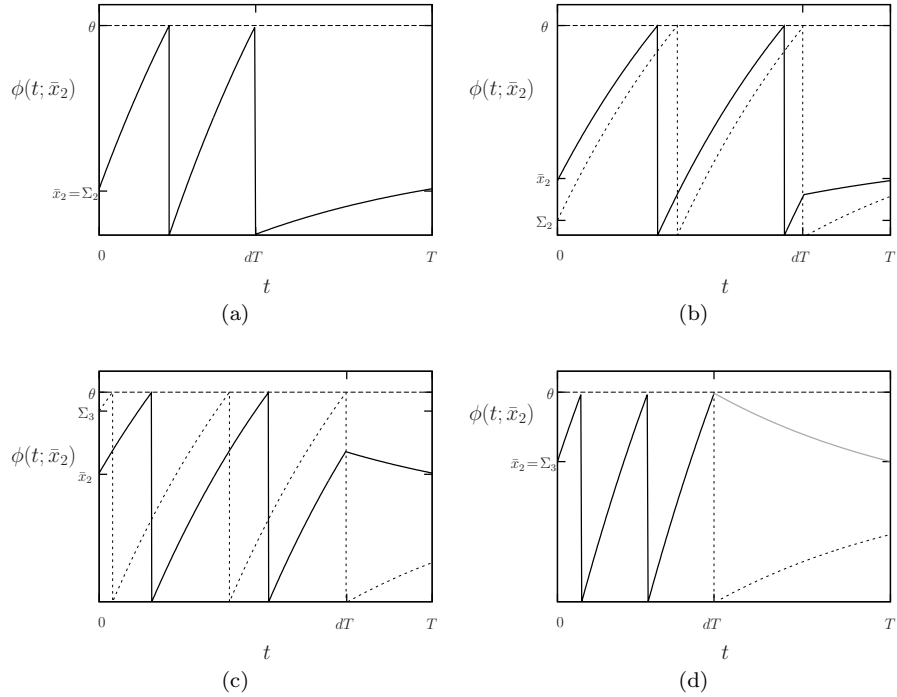


Figure 3.3:  $T$ -periodic orbit spiking twice per period (fixed point  $\bar{x}_2$  of the stroboscopic map). It undergoes border collision bifurcations when it collides with the boundaries  $\Sigma_2$  and  $\Sigma_3$  (a) and (d), respectively. The periodic orbit shown in (d) is its limit when  $\bar{x}_2 \rightarrow \Sigma_3^-$ ; note that for  $\bar{x}_2 = \Sigma_3$  it should be reset to 0 at  $t = dT$ , this is why it is shown in gray. In (b) and (c), the trajectories of these boundaries are shown in dashed lines; note that they collide with the threshold at  $t = dT$ . Parameter values for panel (c) are the same as for point  $D$  of figure 2(a). The four figures are a one to one correspondence with the four figures of figure 3.4, where the stroboscopic map is shown for the same parameter values.

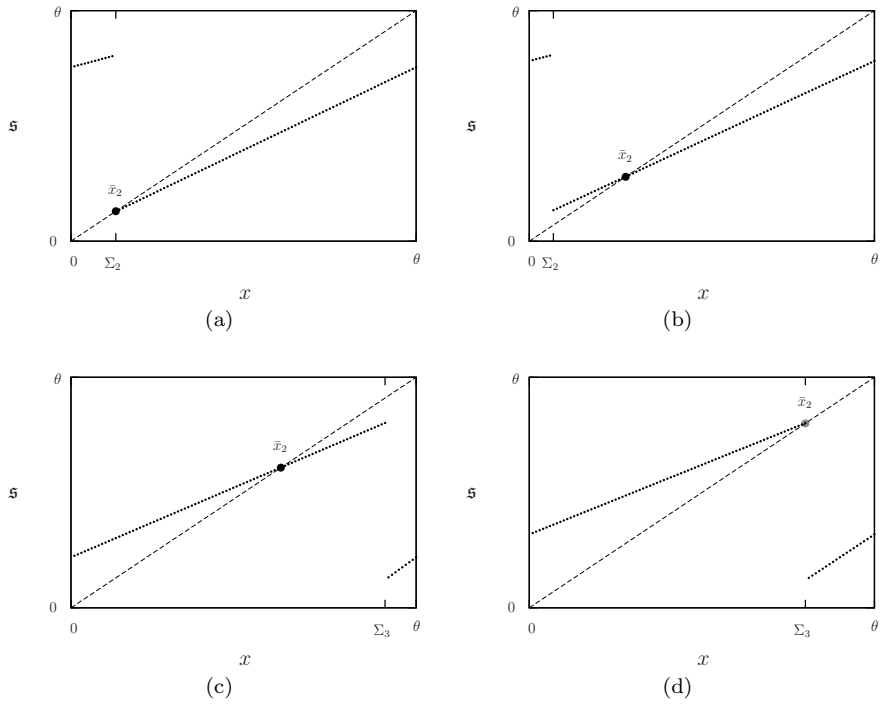


Figure 3.4: Stroboscopic map for the  $T$ -periodic orbits shown in figure 3.3. In (a) and (d) the fixed point  $\bar{x}_2$  undergoes border collision bifurcation when it collides with the boundaries  $\Sigma_2$  from the right and  $\Sigma_3$  from the left, respectively. Note that, in (d) the fixed point is shown in gray to emphasize that the map takes indeed the value on the right for  $x = \Sigma_3$ . In (b)-(c) the boundary  $\Sigma_2$  disappears and a new boundary  $\Sigma_3$  appears while the fixed point  $\bar{x}_2$  remains.

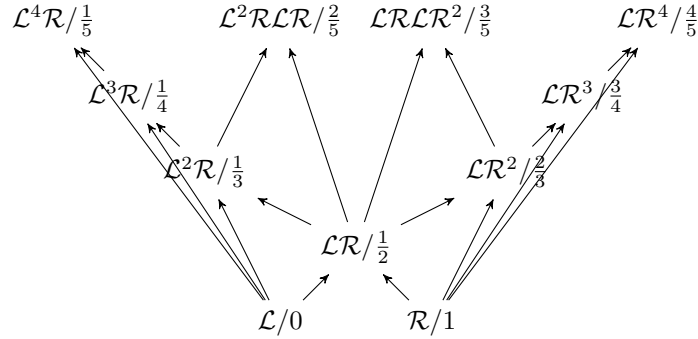


Figure 3.5: Symbolic sequences and rotation numbers forming the so-called Farey tree structure for the period adding. The symbol  $\mathcal{L}$  corresponds to a step on the left of the discontinuity,  $\mathcal{R}$  to a step on its right.

the following reason.

When varying parameters along the line shown in 2(a) inside the gray regions, a new discontinuity  $\Sigma_{n+1}$  enters  $[0, \theta]$  ( $\theta = \Sigma_{n+1}$ ) and  $\Sigma_n$  no longer exists, while the periodic orbit spiking  $n$  times still exists and hence is not subject to any bifurcation (see figures 4(b)-4(c) for  $n = 2$ ). At this moment, however, the rotation number associated with this periodic orbit jumps from 1 to 0, and the state space is now split in two pieces,  $[0, \Sigma_{n+1})$  and  $[\Sigma_{n+1}, \theta)$  where the system spikes  $n$  and  $n + 1$  times, respectively.

**Remark 3.2.** *The symbols  $\mathcal{L}$  and  $\mathcal{R}$  in the symbolic sequences of the periodic orbits located in the white regions correspond to  $n$  and  $n + 1$  spikes in a  $T$ -time interval, respectively.*

**Remark 3.3.** *Following [GIT84], one can relate the rotation numbers to the symbolic dynamics associated with the periodic orbits that appear along the line shown in figure 2(a), by dividing the number of  $\mathcal{R}$ 's that appear in the symbolic sequence by the period of the periodic orbit. Hence, taking into account remark 3.2, between  $B$  and  $C$  in figure 2(a) the rotation number equals the firing-number  $\eta$ .*

**Remark 3.4.** *Beyond point  $C$  in the line shown in fig. 2(a),  $\eta$  varies along the line as the rotation number but without the jumping from 1 to 0. Hence, this quantity follows a devil's staircase from 0 to  $\infty$  when parameters are varied along such a line.*

### 3.2 Bifurcation scenario upon frequency variation

We now focus on how the bifurcation scenario described in §3.1 and schematically shown in figure 3.2 varies with  $T$ .

As proven in [GKC13] this bifurcation scenario does not qualitatively depend

on  $T$  and, hence, no other bifurcations are introduced nor subtracted under variation of  $T$ . However, the shape of the bifurcation curves varies, as the next two propositions show (see figures 4.1 and 4.2 for graphical support through an example). Proposition 3.1 tells us that the bifurcation curves accumulate to the horizontal line  $1/A = 1/Q_c$  when  $T \rightarrow \infty$  (labeled in all paths of figures 4.1 and 4.2). Proposition 3.2 tells us that all bifurcation curves accumulate to horizontal axis, except for the one given by  $A_0(d)$ , which accumulates to the straight line  $1/A = d/Q_c$  (see figure 1(a)).

**Proposition 3.1.** *Let  $d \in (0, 1)$  and consider the values given in definition 3.1,  $A_n^{\mathcal{R}, \mathcal{L}} = A_n^{\mathcal{R}, \mathcal{L}}(d, T)$  and  $A_0 = A_0(d, T)$ , for which the fixed points  $\bar{x}_n$  undergo border collision bifurcations. Then,*

$$\lim_{T \rightarrow \infty} A_0(d, T) = \lim_{T \rightarrow \infty} A_n^{\mathcal{R}}(d, T) = \lim_{T \rightarrow \infty} A_n^{\mathcal{L}}(d, T) = Q_c,$$

where  $Q_c$  is the critical dose defined in (2.11).

*Proof.* Let  $\varphi(t; x; A)$  be the flow associated with system  $\dot{x} = f(x) + A$ , and let  $\bar{x}_n = \bar{x}_n(d, T, A)$  be the initial condition ( $t_0 = 0$ ) for a  $T$ -periodic orbit spiking  $n$  times (fixed point of the stroboscopic map  $\mathfrak{s}(x)$ ). As shown in figure 3.6, (see [GKC13] for more details), the border collision bifurcations that the  $T$ -periodic orbits spiking  $n$  times undergo at  $A = A_n^{\mathcal{R}}(d, T)$  (fig. 6(a)) and  $A = A_n^{\mathcal{L}}(d, T)$  (fig. 6(b)) are characterized by the equations

$$\begin{aligned} \varphi(t_n; \bar{x}_n; A_n^{\mathcal{R}}) &= \theta \\ \varphi(\delta; 0; A_n^{\mathcal{R}}) &= \theta \\ \varphi(T - dT; 0; 0) &= \bar{x}_n \\ t_n + (n - 1)\delta &= dT \end{aligned} \tag{3.1}$$

and

$$\begin{aligned} \varphi(t'_n; \bar{x}_n; A_n^{\mathcal{L}}) &= \theta \\ \varphi(\delta'; 0; A_n^{\mathcal{L}}) &= \theta \\ \varphi(T - dT; \theta; 0) &= \bar{x}_n \\ t'_n + (n - 1)\delta' &= dT, \end{aligned} \tag{3.2}$$

respectively. As  $n$  is fixed, when  $T \rightarrow \infty$  also  $\delta \rightarrow \infty$ . Hence, from equations (3.1) and (3.2) we get that the values  $A = A_n^{\mathcal{R}}$  and  $A = A_n^{\mathcal{L}}(d, T)$  are such that system  $\dot{x} = f(x) + A$  possesses an attracting critical point at  $x = \theta$ . From equation (2.11) we get that the limiting values are  $A_n^{\mathcal{R}} = A_n^{\mathcal{L}} = Q_c$ .

Arguing similarly and using that the bifurcation condition for  $A_0(d, T)$  is equivalent to (3.2), one gets that  $A_0 \rightarrow Q_c$ .  $\square$

**Proposition 3.2.** *Let  $d \in (0, 1)$  and consider the bifurcation values of the fixed points  $\bar{x}_n \in S_n$ ,  $A_0(d, T)$  and  $A_n^{\mathcal{R}, \mathcal{L}}(d, T)$  ( $n > 1$ ) as in definition 3.1. Then they fulfill*

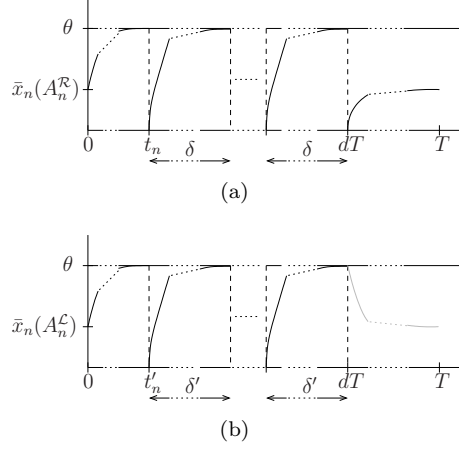


Figure 3.6: Bifurcations of the  $T$ -periodic spiking  $n$  times for large values of  $T$ . (a) and (b) smallest and largest values of  $A$  ( $A_n^{\mathcal{R}}$  and  $A_n^{\mathcal{L}}$ , respectively) for which the  $T$ -periodic orbit exists. This corresponds to the border collision bifurcations given by  $\bar{x}_n(A_n^{\mathcal{R}}) = \Sigma_n$  and  $\bar{x}_n((A_n^{\mathcal{L}})^-) = \Sigma_{n+1}$ , respectively. The gray color in (b) reflects the fact that such orbit does no longer exist for  $A = A_n^{\mathcal{L}}$ , as it must be reset to 0 at  $t = dT$ . The orbit shown is the limiting periodic orbit for  $A \rightarrow A_n^{\mathcal{L}}$ .

i)

$$\lim_{T \rightarrow 0} A_0(d, T) = \frac{Q_c}{d}, \quad (3.3)$$

where  $Q_c$  is the critical dose defined in (2.11).

ii)

$$\lim_{T \rightarrow 0} A_n^{\mathcal{R}, \mathcal{L}}(d, T) = 0, \quad n > 1.$$

*Proof.* Let  $\varphi(t; x; A)$  be the flow associated with the system  $\dot{x} = f(x) + A$ . The fact that  $f(x)$  is a monotonously decreasing function with a simple zero ensures that the bifurcation suffered by the non-spiking  $T$ -periodic orbit will be given when

$$\begin{cases} \varphi(dT; \bar{x}_0; A_0) = \theta \\ \varphi(T - dT; \theta; 0) = \bar{x}_0, \end{cases} \quad (3.4)$$

where  $\bar{x}_0$  is the initial condition for such periodic orbit for  $t = 0$ . We want to solve these equations for  $A_0$  and  $\bar{x}_0$  for a fixed  $d \in (0, 1)$  and  $T > 0$ , and see how this solution behaves when  $T \rightarrow 0$ .

For  $T \rightarrow 0$  we can approximate the flow by a linear one and obtain

$$\begin{aligned} \varphi(dT; x; A_0) &= x + (f(x) + A_0) dT + O(T^2) \\ \varphi(T - dT; \theta; 0) &= \theta + f(\theta)(1 - d)T + O(T^2). \end{aligned}$$



Hence, for  $T \rightarrow 0$ , the bifurcation condition (3.4) becomes equivalent to the system

$$\begin{cases} \bar{x}_0 + (f(\bar{x}_0) + A_0) dT = \theta \\ \theta + f(\theta)(1-d)T = \bar{x}_0, \end{cases}$$

which we can solve explicitly to prove *i*),

$$\lim_{T \rightarrow 0} A_0(d, T) = \frac{Q_c}{d}.$$

Let now  $A_n^{\mathcal{R}}$  and  $A_n^{\mathcal{L}}$  be the values of  $A$  for which a  $T$ -periodic orbits spiking  $n$  times undergo the border collision bifurcation described in § 3.1. Among other conditions, these bifurcations are characterized by the fact that their respective trajectories reach the threshold at  $t \bmod T = dT$  immediately after performing a spike,

$$\varphi(dT; 0; A_n^{\mathcal{R}, \mathcal{L}}) = \theta.$$

Hence, one necessary needs  $A_n^{\mathcal{R}, \mathcal{L}} \rightarrow \infty$  when  $T \rightarrow 0$ , which proves *ii*).  $\square$

**Remark 3.5.** *Note that the fact that the border collision bifurcation curves defined by  $A_n^{\mathcal{R}, \mathcal{L}}$  collapse to the horizontal axis for  $T \rightarrow 0$  implies that all other border collision bifurcation curves separating regions of existence of periodic orbits with higher periods also collapse to the horizontal axis, as they are located in between.*

The next result tells us that all bifurcation curves vary monotonically with  $T$ .

**Lemma 3.1.** *For a fixed  $d \in (0, 1)$  let  $A^{\mathcal{R}}(d, T)$  and  $A^{\mathcal{L}}(d, T)$  be the values for which a periodic orbit undergoes a border collision bifurcation. Then they are monotonous functions of  $T$ .*

*Proof.* We prove the result for the bifurcations undergone by fixed points of the stroboscopic map ( $A_n^{\mathcal{L}}(d, T)$  and  $A_n^{\mathcal{R}}(d, T)$ ). Proceeding similarly one obtains the analogous result for periodic orbits.

Assume that  $\bar{x}_n$  is a fixed point of the stroboscopic map  $\mathfrak{s}(x)$  leading to a  $T$ -periodic orbit exhibiting  $n$  spikes per period. Such a fixed point undergoes a left bifurcation for  $A = A_n^{\mathcal{L}}$  when the following equations are satisfied (see fig. 3(d))

$$\begin{aligned} \int_{\bar{x}_n}^{\theta} \frac{dx}{f(x) + A_n^{\mathcal{L}}} + n \int_0^{\theta} \frac{dx}{f(x) + A_n^{\mathcal{L}}} &= aT \\ \int_{\theta}^{\bar{x}_n} \frac{dx}{f(x)} &= (1-a)T, \end{aligned}$$

where we have renamed the duty cycle  $d$  by  $a$  to avoid the confusion with the notation used for derivatives and differentials. Differentiating the previous

equations with respect to  $T$  we get

$$a = -\frac{dA_n^{\mathcal{L}}}{dT} \left( \int_{\bar{x}_n}^{\theta} \frac{dx}{(f(x) + A_n^{\mathcal{L}})^2} + n \int_0^{\theta} \frac{dx}{(f(x) + A_n^{\mathcal{L}})^2} \right) - \frac{1}{f(\bar{x}_n) + A_n^{\mathcal{L}}} \frac{d\bar{x}_n}{dT}$$

$$\frac{d\bar{x}_n}{dT} = (1-a)f(\bar{x}_n).$$

We want to see that  $dA_n^{\mathcal{L}}/dT < 0$ . Combining these last equations we get

$$-\left( \int_{\bar{x}_n}^{\theta} \frac{dx}{(f(x) + A_n^{\mathcal{L}})^2} + n \int_0^{\theta} \frac{dx}{(f(x) + A_n^{\mathcal{L}})^2} \right) \frac{dA_n^{\mathcal{L}}}{dT} = a + (1-a) \frac{f(\bar{x}_n)}{f(\bar{x}_n) + A_n^{\mathcal{L}}}.$$

We note that

- the coefficient of  $dA_n^{\mathcal{L}}/dT$  in the left hand side is negative
- $f(\bar{x}_n) (f(\bar{x}_n) + A_n^{\mathcal{L}}) < 0$ .

Hence, to prove the result we need to show that

$$a + (1-a) \frac{f(\bar{x}_n)}{f(\bar{x}_n) + A_n^{\mathcal{L}}} > 0. \quad (3.5)$$

We know that if  $T \rightarrow \infty$  then  $f(\bar{x}_n) \rightarrow 0$  and  $A_n^{\mathcal{L}} \rightarrow Q_c$  (proposition 3.1). Hence (3.5) holds for large  $T$ . We will prove that  $a + (1-a)f(\bar{x}_n)/(f(\bar{x}_n) + A) = 0$  is not possible. First note that this equation is equivalent to  $\bar{x}_n = f^{-1}(-aA)$ . Hence we consider the following system of three equations:

$$\int_{\bar{x}_n}^{\theta} \frac{dx}{f(x) + A_n^{\mathcal{L}}} + n \int_0^{\theta} \frac{dx}{f(x) + A_n^{\mathcal{L}}} = aT$$

$$\int_{\theta}^{\bar{x}_n} \frac{dx}{f(x)} = (1-a)T \quad (3.6)$$

$$\bar{x}_n = f^{-1}(-aA_n^{\mathcal{L}}).$$

and we show that the three equations in (3.6) cannot be simultaneously satisfied. Eliminating the variables we get

$$\int_{f^{-1}(-aA_n^{\mathcal{L}})}^{\theta} \left( \frac{a}{f(x)} + \frac{1-a}{f(x) + A_n^{\mathcal{L}}} \right) dx + n \int_0^{\theta} \frac{(1-a)}{f(x) + A_n^{\mathcal{L}}} dx = 0.$$

We know that  $0 < -f(\theta) \leq A_n^{\mathcal{L}} < -f(\theta)/a$ . We define the function

$$\psi(A) = \int_{f^{-1}(-aA)}^{\theta} \left( \frac{a}{f(x)} + \frac{1-a}{f(x) + A} \right) dx + n \int_0^{\theta} \frac{(1-a)}{f(x) + A} dx.$$

Clearly  $\psi(-f(\theta)/a) > 0$ . We compute

$$\begin{aligned}\psi'(A) &= \frac{a}{f'(f^{-1}(-aA))} \left( -\frac{1}{A} + \frac{1}{A} \right) - \int_{f^{-1}(-aA)}^{\theta} \frac{1-a}{(f(x)+A)^2} dx \\ &\quad - n \int_0^{\theta} \frac{1-a}{(f(x)+A)^2} dx \\ &= - \int_{f^{-1}(-aA)}^{\theta} \frac{1-a}{(f(x)+A)^2} dx - n \int_0^{\theta} \frac{1-a}{(f(x)+A)^2} dx < 0.\end{aligned}$$

Hence  $\psi$  is strictly monotonic so it cannot have a 0 in  $[-f(\theta), -f(\theta)/a]$ .

We now show that the same holds for the right bifurcations of the fixed points (see fig. 3(a)); that is,  $dA_n^{\mathcal{R}}/dT < 0$ .

In this case, the equations that determine such bifurcation become

$$\begin{aligned}\int_{\bar{x}_n}^{\theta} \frac{dx}{f(x) + A_n^{\mathcal{R}}} + n \int_0^{\theta} \frac{dx}{f(x) + A_n^{\mathcal{R}}} &= aT \\ \int_0^{\bar{x}_n} \frac{dx}{f(x)} &= (1-a)T,\end{aligned}$$

Unlike in the previous case,  $\bar{x}_n$  increases to  $\bar{x}$  when  $T$  is increased. This leads to a decrease of the time of the first spike (value of the first integral). Hence, one necessary needs to decrease  $A_n^{\mathcal{R}}$  in order to keep these equations satisfied.  $\square$

We will now use propositions 3.1 and 3.2 to derive information about the behavior of the firing rate for large and small periods, propositions 3.3 and 3.4, respectively. First we present the next corollary of propositions 3.1, 3.2 and lemma 3.1. It provides a partition of the parameter space in three different regions regarding spiking properties for different values of  $T$ .

**Corollary 3.1.** *The parameter space  $d \times 1/A$  is divided in three main regions with the following properties*

- Non-spiking region,

$$\{(d, 1/A) \in \mathbb{R}^2 \mid d \in (0, 1), A < Q_c\}, \quad (3.7)$$

*for which the corresponding periodic orbit does not contain any spike for any  $d \in (0, 1)$  and  $T > 0$ .*

- Permanent-spiking region,

$$\{(d, 1/A) \in \mathbb{R}^2 \mid d \in (0, 1), A > Q_c/d\}, \quad (3.8)$$

*for which, the existing periodic orbit contains spikes for all  $T > 0$ .*

- Conditional-spiking region,

$$\{(d, 1/A) \in \mathbb{R}^2 \mid d \in (0, 1), Q_c < A < Q_c/d\}, \quad (3.9)$$

for which there exists  $T_0 > 0$  such that the corresponding periodic orbit contains spikes if  $T > T_0$  and does not if  $T < T_0$ .

**Remark 3.6.** *The spiking-region is formed by the union of the conditional and permanent-spiking regions.*

**Corollary 3.2.** *If  $(d, 1/A)$  belongs to the spiking-region, then the firing rate  $r(T)$  follows a devil's staircase with monotonically decreasing steps.*

*Proof.* It follows from propositions 3.1, 3.2 and lemma 3.1 that the bifurcation lines defining the steps of the devil's staircase move up monotonically as  $T$  is increased. Hence, if we fix  $(d, 1/A)$  in the spiking region, then as  $T$  increases all the bifurcation curves pass through the point  $(d, 1/A)$  and the bifurcation diagram is the same as when  $d$  and  $T$  are fixed and  $A$  is varied (i.e. when varying parameters along the line shown in fig. 2(a) for a fixed  $T$ ).

Recall that the devil's staircase followed by the rotation number is constant along the steps. Then, using remarks 3.3 and 3.4 and formula (2.9) we conclude that  $r(T)$  follows a devil's staircase which is monotonically decreasing along the steps.  $\square$

From the previous results we get the next corollary providing the behaviour of the firing number  $\eta$  for large and small values of  $T$ .

**Corollary 3.3.** *In the spiking region the firing number defined in 2.2 (average number of spikes per period of the stroboscopic map) satisfies*

$$\begin{aligned} \lim_{T \rightarrow 0} \eta(T) &= 0 \\ \lim_{T \rightarrow \infty} \eta(T) &= \infty. \end{aligned}$$

Moreover, in the conditional spiking region  $\eta(T) = 0$  for  $0 < T < T_0 = T_0(A, d)$ .

Note that the relation between the firing number and firing rate given by equation (2.9) implies that their asymptotic behavior is not necessarily the same when  $T \rightarrow \infty$  or  $T \rightarrow 0$ . We will now use the results obtained so far in this section to characterize the limits of the firing rate as  $T \rightarrow \infty$  and as  $T \rightarrow 0$ . The following result describes the limit of  $r(T)$  as  $T \rightarrow \infty$  for points in the spiking region.

**Proposition 3.3.** *Let  $(d, 1/A)$  belong to the spiking-region ( $d \in (0, 1)$  and  $A > Q_c$ ) and let  $\varphi(t; x; A)$  be the flow associated with  $\dot{x} = f(x) + A$ . Let  $\delta > 0$  be the smallest such that*

$$\varphi(\delta; 0; A) = \theta.$$

Then, the firing rate satisfies

$$\lim_{T \rightarrow \infty} r(T) = \frac{d}{\delta}.$$

*Proof.* We will show that the devil's staircase followed by the firing number  $\eta(T)$  converges to a common discontinuous staircase whose each step has length  $\delta/d$ . These steps have integer values,  $n$ , and correspond to  $T$ -periodic orbits spiking  $n$  times. More specifically, we prove that

$$\lim_{T \rightarrow \infty} \eta(T) - E\left(\frac{\delta T}{d}\right) \rightarrow 0, \quad (3.10)$$

where  $E(x)$  is the integer value of  $x$ . The result follows from (3.10) and from the definition of firing rate.

To prove (3.10) we focus on a  $T$ -periodic orbit with  $n$  spikes per period. Let  $\bar{x}_n(T)$  be the initial condition ( $t_0 = 0$ ) for such an orbit (fixed point of the stroboscopic map). This fulfills

$$\begin{aligned} \varphi(t_n; \bar{x}_n(T); A) &= \theta \\ \varphi(dT - (n-1)\delta - t_1; 0; A) &= x' \\ \varphi(T - dT; x'; 0) &= \bar{x}_n(T), \end{aligned}$$

for some  $0 < t_n < \delta$ . The last equation tells us that

$$\lim_{T \rightarrow \infty} \bar{x}_n(T) = \bar{x}, \quad (3.11)$$

where  $\bar{x}$  is the equilibrium point (2.5) associated with system  $\dot{x} = f(x)$  given by assumptions H.1-H.2.

At the same time, this tells us that the stroboscopic map converges to a constant function equal to  $\bar{x}$ . Recalling that the discontinuities of the stroboscopic map occur at  $x = \Sigma_i$ , the gaps at these discontinuities tend to zero,

$$\lim_{T \rightarrow \infty} \mathfrak{s}(\Sigma_n^-) = \lim_{T \rightarrow \infty} \mathfrak{s}(\Sigma_n^+) = \bar{x}.$$

Hence, when  $T \rightarrow \infty$  there is no space for periodic orbits with higher periods. In other words, let  $T_n^{\mathcal{R}}$  and  $T_n^{\mathcal{L}}$  be the values of  $T$  for which a  $T$ -periodic orbit spiking  $n$  times appears and disappears through border collisions bifurcations, respectively (figures 7(a) and 7(c), respectively). Then we have that

$$\lim_{T \rightarrow \infty} T_{n+1}^{\mathcal{R}} - T_n^{\mathcal{L}} = 0,$$

and the devil's staircase converges to be a common staircase. Its steps are given by integer values  $n$ , as they correspond to the firing-number associated with  $T$ -periodic orbits spiking  $n$  times.

We now estimate the length of these steps when  $T \rightarrow \infty$ . From equation (3.11) we get that, as  $T \rightarrow \infty$ ,  $t_1$  converges to the solution of the equation

$$\varphi(t_1; \bar{x}; A) = \theta. \quad (3.12)$$

As the number of spikes performed by a  $T$ -periodic orbit tends to infinity as  $T \rightarrow \infty$  (proposition 3.1), the interval of time where the spikes occur is of order

$n\delta$ . Hence, taking into account the characteristics of the  $T$ -periodic orbit at its bifurcation (see figures 7(c), 7(a) and [GKC13]), we get

$$\begin{aligned}dT_n^{\mathcal{R}} &\sim n\delta \\dT_n^{\mathcal{L}} &\sim (n+1)\delta,\end{aligned}$$

and thus

$$T_n^{\mathcal{L}} - T_n^{\mathcal{R}} \sim \frac{\delta}{d},$$

which is the length of the step with integer value.  $\square$

We end this section with a result which describes the behavior of  $r(T)$  as  $T \rightarrow 0$ .

**Proposition 3.4.** *Let  $(d, 1/A)$  belong to the spiking-region, and let*

$$\dot{x} = f(x) + Ad \tag{3.13}$$

*be the averaged version of system (2.1). Let  $\hat{\varphi}(t; x)$  be its associated flow and let  $\hat{\delta} > 0$  be the least number such that*

$$\hat{\varphi}(\hat{\delta}; 0) = \theta. \tag{3.14}$$

*Then,*

- *if  $(d, 1/A)$  belongs to the conditional-spiking region ( $Ad < Q_c$ ) then  $r(T) = 0$  if  $T < T_0$ , where  $T_0$  is given in corollary 3.1,*
- *if  $(d, 1/A)$  belongs to the permanent-spiking region ( $Ad > Q_c$ ), then*

$$\lim_{T \rightarrow 0} r(T) = \frac{1}{\hat{\delta}}.$$

*Proof.* For the first case we use corollary 3.1, from which we get that, if  $T < T_0$  then  $\eta(T) = 0$ , and hence  $r(T) = 0$ .

For the second case we study how the devil's staircase  $r(T)$  behaves when  $T \rightarrow 0$ . Note that, when  $r(T) < 1$ , this one coincides with the rotation number of the periodic orbits found when varying  $T$  (see remark 3.3).

Using that  $\lim_{T \rightarrow 0} \eta(T) = 0$ , we get that, for any  $T$  small enough, we can find  $n$  large enough such that

$$\frac{1}{n+1} \leq \eta(T) \leq \frac{1}{n}.$$

Hence, as  $1/n - 1/(n+1) \rightarrow 0$ , this is enough to study how the steps given by the rotation numbers of the form  $1/n$  behave. Taking into account that the symbolic dynamics is organized by a Farey tree structure (a one to one mapping with the rotation numbers), this rotation numbers are associated with periodic orbits with symbolic sequences of the form  $\mathcal{L}^n \mathcal{R}$ . These periodic orbits are

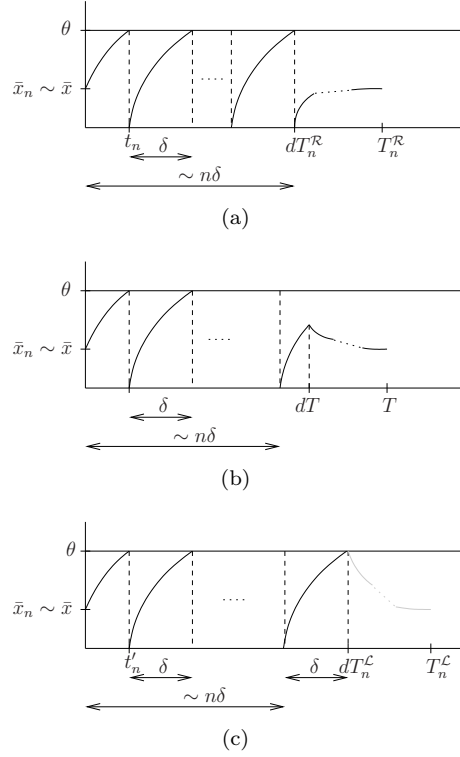


Figure 3.7:  $T$ -periodic orbit spiking  $n$  times at its bifurcations for large values of  $T$ . The periodic orbit appears (a) and disappears (c) through border collision bifurcations at  $T = T_n^{\mathcal{R}}$  and  $T = T_n^{\mathcal{L}}$ , respectively. In (b) a  $T$ -periodic orbit for  $T \in (T_n^{\mathcal{R}}, T_n^{\mathcal{L}})$ . The gray color emphasizes the fact that the periodic orbit does not exist for  $T = T_n^{\mathcal{L}}$  as it should be reset to 0 when the threshold is reached. The orbit shown is the limiting periodic orbit when  $T \rightarrow (T_n^{\mathcal{L}})^-$ . In all three cases the fixed point  $\bar{x}_n$  approaches  $\bar{x}$ , the critical point of system (2.4) as  $T \rightarrow \infty$ .

characterized by exhibiting one spike after  $n$  iterations of the stroboscopic map, and are determined by the equations

$$\begin{aligned}
\varphi(dT; \bar{x}_{\mathcal{L}^n \mathcal{R}}; A) &= x_1 \\
\varphi(T - dT; x_1; 0) &= x'_1 \\
\varphi(dT; x'_1; A) &= x_2 \\
\varphi(T - dT; x_2; 0) &= x'_2 \\
&\vdots \\
\varphi(t'; x'_n; A) &= \theta \\
\varphi(dT - t'; 0; A) &= x_{n+1} \\
\varphi(T - dT; x_{n+1}; 0) &= \bar{x}_{\mathcal{L}^n \mathcal{R}},
\end{aligned}$$

where  $\varphi(t; x; A)$  is the flow associated with system  $\dot{x} = f(x) + A$  and  $\bar{x}_{\mathcal{L}^n \mathcal{R}}$  is the initial condition for the  $\mathcal{L}^n \mathcal{R}$  periodic orbit for  $t_0 = 0$ . From the two last equations, we get that  $\lim_{T \rightarrow 0} \bar{x}_{\mathcal{L}^n \mathcal{R}} = 0$ .

After applying a time rescaling, the original system (2.1) and its averaged version become

$$\dot{x} = T \left( f(x) + \tilde{I}(t) \right) \quad (3.15)$$

$$\dot{x} = T (f(x) + Ad), \quad (3.16)$$

where  $\tilde{I}(t)$  is now 1-periodic. We now consider solutions of systems (3.15) and (3.16) with  $O(T)$  close initial conditions. The averaging theorem of Bogoliubov and Mitropolski [BM61] tells us that, if  $T$  is small enough, then such solutions remain  $O(T)$ -close for a  $t \sim 1/T$  time scale provided that they have not reached the threshold. Note that the result given in [BM61] applies because it does not require continuity in  $t$  but boundedness and Lipschitz in  $x$ .

Hence, letting  $\hat{\varphi}(t; x)$  be the flow of the averaged system (3.13), if  $T$  is small enough we have that

$$\varphi(T - dT; \varphi(dT; x; A); 0) = \hat{\varphi}(T; x) + O(T).$$

Hence, as long as the threshold is not reached, we can approximate the real flow by the averaged one. Using that  $\bar{x}_{\mathcal{L}^n \mathcal{R}} \rightarrow 0$  when  $T \rightarrow 0$ , the time taken by the real flow to reach the threshold  $x = \theta$  from  $x = \bar{x}_{\mathcal{L}^n \mathcal{R}}$  approaches  $\hat{\delta}$ :

$$nT + t' \rightarrow \hat{\delta}.$$

Hence, as  $t' < dT$ ,  $n$  grows like  $\hat{\delta}/T$  when  $T \rightarrow 0$  and thus

$$\lim_{T \rightarrow 0} r(T) = \lim_{T \rightarrow 0} \frac{1}{nT} = \frac{1}{\hat{\delta}}.$$

□



**Remark 3.7.** Note that equation (3.14) has sense only if the averaged system (3.13) has a stable critical point above the threshold, which occurs if  $Ad > Q_c$ . This occurs only in the permanent-spiking region.

**Remark 3.8.** From proposition 3.2 we get that the value of the firing rate for small frequencies depends on the released dose  $Ad$ , the average of  $I(t)$ . However, for large values of  $T$  (proposition 3.1), it depends explicitey on  $A$  and  $d$ .

### 3.3 Optimization of the firing rate

As shown in corollary 3.2, the firing rate as a function of  $T$ , the period of the forcing  $I(t)$ , follows a devil's staircase with monotonically decreasing pieces (see figure 2.1). Each of these pieces occurs in a  $T$ -interval,  $(T_\sigma^{\mathcal{R}}, T_\sigma^{\mathcal{L}})$ , for which a unique periodic orbit  $\sigma$  exists. Hence, the firing rate exhibits local maxima at  $T = T_\sigma^{\mathcal{R}}$ , and local minima at  $T = T_\sigma^{\mathcal{L}}$ . As a consequence of this there exists an infinite number of local minima and maxima at any interval of the form  $(T_\sigma^{\mathcal{L}}, T_\gamma^{\mathcal{R}})$ , with  $\sigma$  and  $\gamma$  meaning different periodic orbits.

Of particular interest is when  $\sigma$  and  $\gamma$  are consecutive fixed points (spiking  $n$  and  $n+1$  times). In this case, the firing rate in the frequency range corresponding to  $(T_n^{\mathcal{L}}, T_{n+1}^{\mathcal{L}})$  follows a devil's staircase with monotonically decreasing steps but whose envelope is bell shaped; that is, it increases from  $T_n^{\mathcal{L}}$  to  $T_{n+1}^{\mathcal{R}}$ , where it exhibits an absolute maximum, and then decreases to  $T_{n+1}^{\mathcal{L}}$  (see fig. 3.8). Note that the bifurcation values  $T_n^{\mathcal{L}}$ ,  $T_{n+1}^{\mathcal{R}}$  and  $T_{n+1}^{\mathcal{L}}$  can be easily found numerically (by solving equations (3.1) and (3.2) for  $T$ ) and that the values of the firing rate at these values become  $n/T_n^{\mathcal{L}}$ ,  $(n+1)/T_{n+1}^{\mathcal{R}}$  and  $(n+1)/T_{n+1}^{\mathcal{L}}$ , respectively. In real applications one is usually restricted to a bounded range of realistic frequencies for which one observes an absolute maximum of the firing rate (see for example [KJSC97, DHO<sup>+</sup>89]). Hence, this approach could be applied to properly tune system parameters in order to make the model exhibit such a behavior for the desired values of  $T$ .

We now investigate the optimization of the firing rate in the whole range of periods,  $(0, \infty)$ .

Due to the fact that the firing rate is bounded and continuous for  $T > 0$ , it must exhibit a global maximum provided that it is increasing for  $T = 0^+$ . From the argument above, it must occur at some value of the form  $T_\sigma^{\mathcal{R}}$ , respectively, for some periodic orbit  $\sigma$ . The next result tells us that, in general, this periodic orbit will be the  $T$ -periodic orbit spiking once per period.

**Proposition 3.5.** Let  $(d, A)$  be in the spiking region (see remark 3.6), and let  $T_1^{\mathcal{R}}$  and  $T_1^{\mathcal{L}}$  be the values of  $T$  for which the periodic orbit spiking once per period undergoes right and left border collision. Then, there exists some  $\gamma > 0$  such that, if  $T_1^{\mathcal{R}} > \gamma$  then the firing rate  $r(T)$  has global maximum at  $T = T_1^{\mathcal{R}}$ .

*Proof.* Let  $T_n^{\mathcal{R}, \mathcal{L}}$  be the values of  $T$  for which a  $T$ -periodic orbit spiking  $n$  times undergoes border collision bifurcation on the right and left, respectively. As we know, the firing-number is a monotonically increasing function from  $T_n^{\mathcal{L}}$  to  $T_{n+1}^{\mathcal{R}}$ , for any  $n$ . Hence, the maximum must occur for some  $T_n^{\mathcal{R}}$ , right border

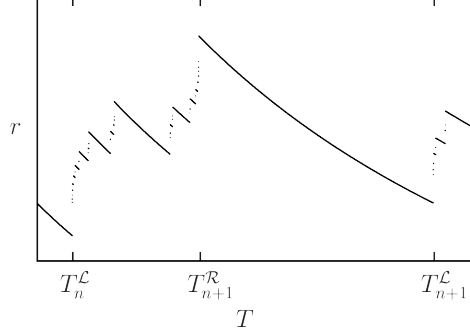


Figure 3.8: Typical response of the firing rate between two consecutive fixed points. Its envelope is bell shaped, exhibiting a maximum at  $T = T_{n+1}^R$ .

collision bifurcation of the  $T$ -periodic orbit spiking  $n$  times (see figure 3(a) for  $n = 2$ ).

Taking into account relation (2.9) and recalling that the firing number for such orbits is  $n$ , the number of spikes, it will be enough to show that

$$\frac{1}{T_1^R} > \frac{2}{T_2^R} > \frac{3}{T_3^R} \cdots,$$

if  $T_1^R$  is large enough in order to see that this periodic orbit spikes once per period.

Let  $\varphi(t; x_0; A)$  and  $\delta > 0$  be as in proposition 3.3, and let  $\bar{x}_n$  be the fixed point of the stroboscopic map leading to the  $T$ -periodic orbit spiking  $n$  times. Then  $T_n^R$  is determined by the following equations (see figure 3(a) for  $n = 2$ )

$$\begin{aligned} \varphi(t_n; \bar{x}_n; A) &= \theta \\ \varphi(T_n^R - dT_n^R; 0; 0) &= \bar{x}_n \\ t_n + (n-1)\delta &= dT_n^R. \end{aligned}$$

As  $T_{n+1}^R > T_n^R$ , recalling that the flow  $\varphi(t; x_0; 0)$  is exponentially attracted by the equilibrium point  $\bar{x}_n$ , from the second equation it comes that, at the moment of the bifurcation

$$\begin{aligned} \bar{x}_n < \bar{x}_{n+1} &\rightarrow \bar{x} \\ t_n > t_{n+1} &\rightarrow \bar{t}, \end{aligned}$$

where  $\bar{t}$  is the smallest such that  $\varphi(\bar{t}; \bar{x}; A) = \theta$ .

As these series converge exponentially (due to the hyperbolicity of  $\bar{x}$ ), we have that there exists some  $N > 0$ ,  $0 < \lambda < 1$  and  $K > 0$  such that

$$n \underbrace{(t_n - t_{n+1})}_{< K\lambda^n} + t_n \rightarrow \bar{t}, \quad n > N. \quad (3.17)$$

Assuming  $n > N$  large enough and using that  $\delta > \bar{t}$  we get

$$\delta > n(t_n - t_{n+1}) + t_n \iff nt_{n+1} + \delta > (n+1)t_n \quad (3.18)$$

$$\iff n \overbrace{(t_{n+1} + n\delta)}^{T_{n+1}^{\mathcal{R}}} > (n+1) \overbrace{(t_n + (n-1)\delta)}^{T_n^{\mathcal{R}}} \quad (3.19)$$

$$\iff \frac{n}{T_n^{\mathcal{R}}} > \frac{n+1}{T_{n+1}^{\mathcal{R}}}. \quad (3.20)$$

In particular, if  $T_1^{\mathcal{R}}$  is large enough,  $\bar{x}_1$  is close enough to  $\bar{x}$  to fulfill (3.17) and (3.18) for  $n = 1$ .  $\square$

**Remark 3.9.** Note that,  $T_1^{\mathcal{R}}$  will be large enough if  $\bar{x}$  is attracting enough.

**Remark 3.10.** Arguing similarly, the global minimum will be the minimum of 0 (if  $(d, A)$  belongs to the conditional spiking region),  $1/\hat{\delta}$  (proposition 3.4) and  $1/T_1^{\mathcal{L}}$ . Note that if the minimum corresponds to  $1/\hat{\delta}$ , then it technically does not exist, as  $T = 0$  is excluded from the domain.

**Corollary 3.4.** For a given system (2.1)-(2.3), the globally maximal firing rate is achieved with the combination of period  $T$ , dose  $Q$ , amplitude  $A$  and duty cycle  $d$  such that the straight line  $1/A = 1/Qd$  is tangent to the bifurcation curve  $A = A_n^{\mathcal{R}}(d)$  for the smallest possible value of  $T$ .

## 4 Example

In this section we use the results presented so far to study the behavior of the firing rate under frequency variation for different configurations. For the sake of simplicity, we choose to study such configurations for a linear system, as it will permit us to compute explicitly the quantities involved in the results of section 3.2. However, we emphasize that these quantities are straight forward to compute numerically for other type of systems for which conditions H.1-H.2 hold.

### 4.1 Linear integrate and fire model

Let

$$f(x) = ax + b. \quad (4.1)$$

In order to satisfy conditions H.1-H.2, we require that  $a < 0$  and  $\bar{x} = -b/a \in (0, \theta)$ , where  $x = \theta$  is the threshold of the integrate and fire system (2.1)-(2.3).

For system (2.1)-(2.3)-(4.1), the critical dose (2.11) becomes

$$Q_c = -\frac{b}{a\theta},$$

which is the minimal amplitude of the pulse (2.2) for which the system (2.1)-(2.3)-(4.1) can exhibit spikes.

The linearity of the system permits us to also explicitly compute the quantity  $\delta$  involved in proposition 3.3,

$$\delta = \frac{1}{a} \ln \left( \frac{\theta a}{b + A} + 1 \right). \quad (4.2)$$

The averaged version of system (2.1)-(2.3)-(4.1) becomes  $\dot{x} = f(x) + Ad$ , for which we can also explicitly compute the quantity  $\hat{\delta}$  involved in proposition 3.4,

$$\hat{\delta} = \frac{1}{a} \ln \left( \frac{\theta a}{b + Ad} + 1 \right).$$

In figures 4.1 and 4.2 we show the bifurcation scenario in the  $d \times 1/A$  parameter space for different values of  $T$ .

As predicted by proposition 3.2, when  $T \rightarrow 0$  the first bifurcation curve,  $A_0$ , tends to be the straight line  $1/A = 1/Q_c d$ , and the rest of bifurcation curves accumulate at  $1/A = 0$  (see figure 4.1).

By contrast, when  $T \rightarrow \infty$ , all bifurcation curves accumulate at the horizontal curve  $1/A = 1/Q_c$ , as predicted by proposition 3.1 (see figure 4.2).

We are now interested in studying the firing rate  $r$  (2.9) under frequency variation. However, when varying the period of the pulse (2.2), we will restrict ourselves to pulses with constant average (constant released dose or energy)  $Q$  given in equation (2.10).

Obviously, the output of the system will be sensitive to variations of the injected energy (dose). Hence, in order to perform an analysis based exclusively on frequency variation we will be interested in the variation of the frequency of the stimulus while keeping the dose constant (dose conservation).

Note that points in the parameter space  $d \times 1/A$  with a fixed dose are located in the straight lines

$$\frac{1}{A} = \frac{1}{Q} d.$$

In figures 4.1 and 4.2 we have highlighted parameter values associated to two different doses. These are given by two different white straight lines; the one with the larger slope ( $Q < Q_c$ ) is fully contained in the non-spiking region when  $T$  small enough, while the other one is contained in the spiking region for all values of  $T$ , and they will lead to different qualitative responses.

Note that the dose conservation can be performed in three different ways in order to keep the quantity  $Q = Ad$  constant. In the first one one varies the duration of the impulse  $\Delta = dT$  as the period  $T$  of the periodic input  $I(t)$  varies, while its amplitude  $A$  is kept constant. This is done by keeping the duty cycle  $d$  constant.

In the second one, the duration of the pulse is fixed, and one varies its amplitude when  $T$  is varied in order to keep constant the average of  $I(t)$ .

Of course, one can also simultaneously vary both magnitudes, giving rise to any different types of parametrizations with respect to  $T$  of the straight lines corresponding to fixed dose.

In the next sections we separately study the first two cases.

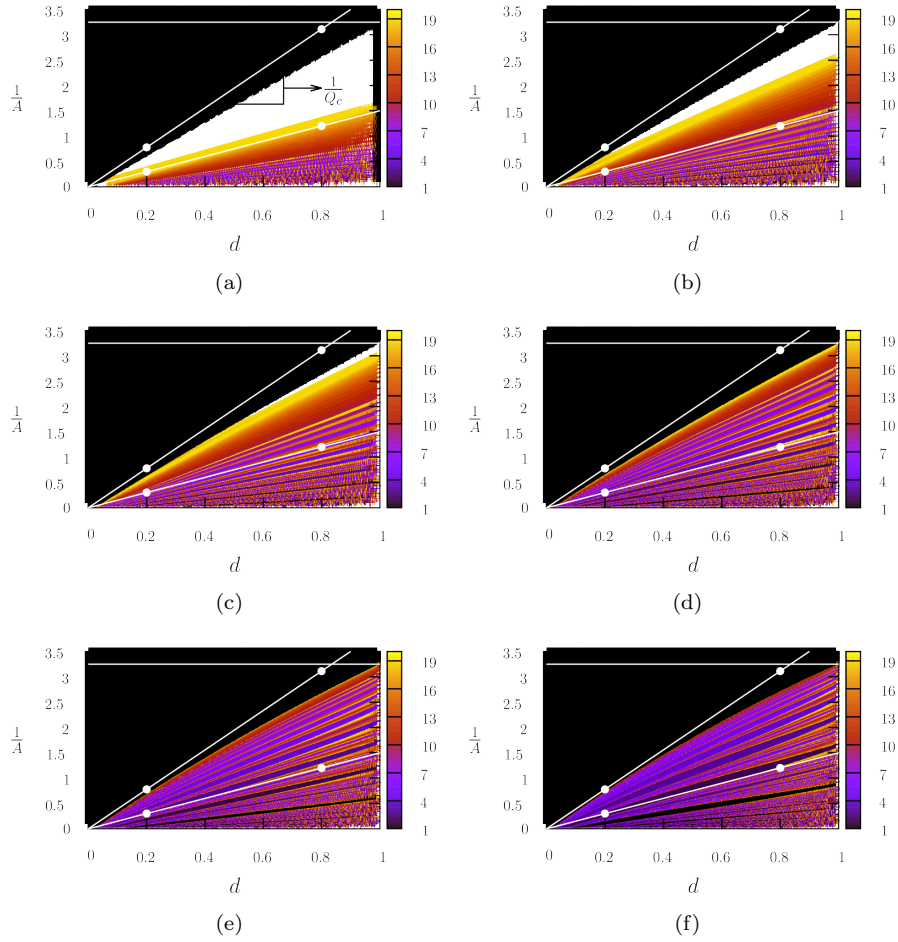


Figure 4.1: Bifurcation scenarios for  $T = 0.1$  (a),  $T = 0.2$  (b),  $T = 0.3$  (c),  $T = 0.5$  (d),  $T = 0.7$  (e) and  $T = 1$  (f), for  $\theta = 1$ ,  $b = 0.2$ ,  $a = -0.5$ . For clarity reasons only periods lower than 20 are shown; regions with higher periods are filled in white. The horizontal line ( $1/A = 1/Q_c$ ) separates the non-spiking and the spiking regions. The straight line with slope  $1/Q_c$  labeled in (a) separates the permanent and conditional spiking regions.

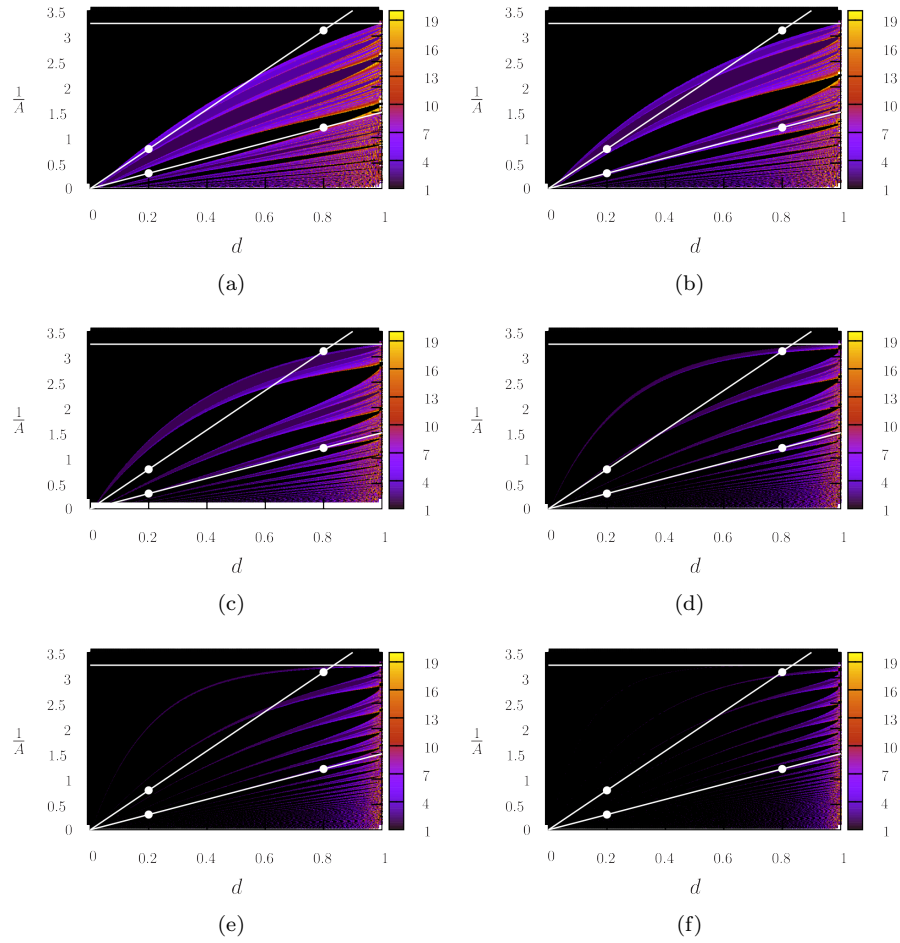


Figure 4.2: Bifurcation scenarios for  $T = 2$  (a),  $T = 3$  (b),  $T = 5$  (c),  $T = 8$  (d),  $T = 10$  (e) and  $T = 15$  (f).

## 4.2 Fixed dose for constant impulse amplitude (width correction)

Taking into account that  $1/A = 1/Qd$ , for a fixed value of the amplitude of the pulse it is enough to keep the duty cycle  $d$  constant in order to obtain an input with constant dose  $Q$ . Hence, in this first approach, we just fix one point in the parameter space  $(d, 1/A)$  and vary  $T$ . This will allow us to directly apply the results shown in § 3.2.

In figure 4.3 we focus on two points in the parameter space located at the white straight line with lower slope (higher dose,  $Q > Q_c$ ), and we show the firing-number,  $\eta$ , (left figures) and the firing rate,  $r$ , (right figures) of the periodic orbits found when varying  $T$ .

As announced in corollary 3.1, as  $Q > Q_c$  these two points in the parameter space are located in the permanent-spiking region and, hence, as mentioned in corollary 3.3, the firing-number tends to zero when  $T \rightarrow 0$ . However, as predicted by proposition 3.4, the firing rate fulfills

$$\lim_{T \rightarrow 0} r(T) = \frac{1}{\hat{\delta}},$$

with  $1/\hat{\delta} = 0.58$  for the used parameter values. As noted in remark 3.7, this value only depends on  $Q$  and hence it is the same for all points with equal dose.

In figure 4.4 we show a magnification of the firing rate for small values of  $T$ , where one can clearly see the structure given by the devil's staircase.

On the other hand, proposition 3.3 provides the limiting value for the firing rate,

$$\lim_{T \rightarrow \infty} r(T) = \frac{d}{\delta},$$

where  $\delta$  is given in (4.2). Note that this quantity depends on  $A$  and, hence, it is different for the two considered case although they correspond to inputs with the same average. For  $(d, 1/A) = (0.2, 0.3)$  (figure 4.3 (b)) we get  $d/\delta = 0.655$ , and for  $(d, 1/A) = (0.8, 1.2)$  we obtain  $d/\delta = 0.604$ .

Finally, observe that the firing rate possesses a global maximum and minimum at  $T = T_1^R$  and  $T = T_1^L$ , respectively, as  $\bar{x}$  is attracting enough.

We now focus on two different inputs with average lower than the critical dose. In figure 4.5 we show the same results for the two points labeled in figures 4.1 and 4.2 located on the white straight line with higher slope (lower dose). For large values of  $T$  the firing rate shows the same behavior as before with limiting values  $d/\delta = 0.244$  (figure 4.5 (b)) and  $d/\delta = 0.125$  (figure 4.5 (d)). However, as predicted in corollary 3.3, unlike in the previous case, as these two points are now located in the conditional-spiking region, there exists some values of  $T$  below which the firing rates vanish.

Note that, as in the previous case, the firing rate exhibits a global maximum at  $T = T_1^R$ . However, the global minimum becomes now 0 for all  $0 < T < T_0$ , as  $(d, A)$  belongs to the conditional spiking region (see remark 3.10).

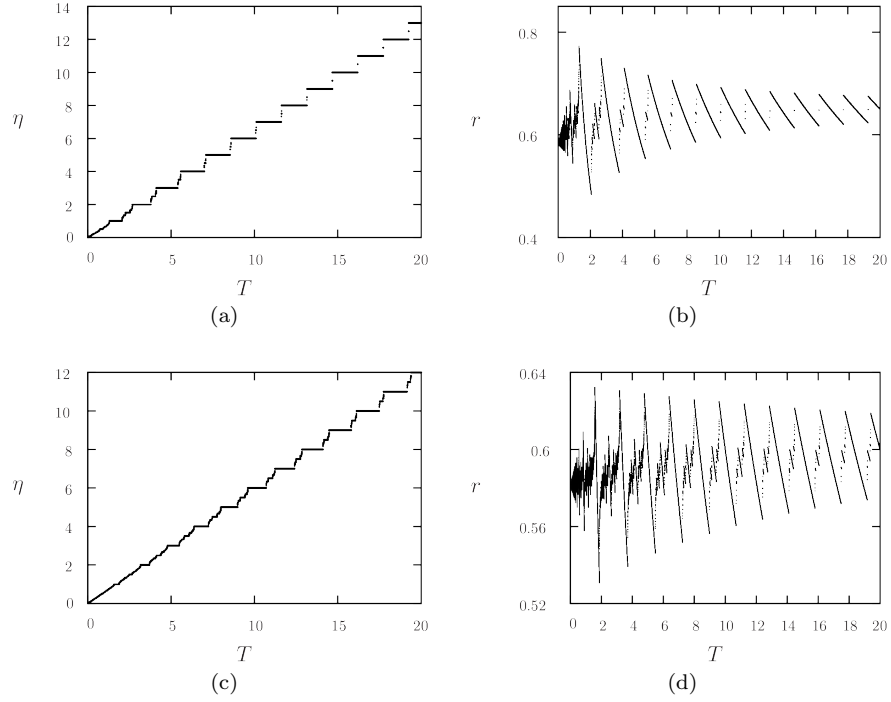


Figure 4.3: Firing-number  $\eta(T)$  (left) and firing rate  $r = \eta(T)/T$  (right), under variation of  $T$  for  $Q = 0.666$ . (a) and (b)  $d = 0.2$  and  $1/A = 0.3$ . (c) and (d)  $d = 0.8$  and  $1/A = 1.2$ . The firing rate follows a devil's staircase with monotonically decreasing pieces exhibiting a maximum at  $T = T_1^{\mathcal{R}}$  and a minimum at  $T = T_1^{\mathcal{L}}$ . Parameters  $a$ ,  $b$  and  $\theta$  are set as in figure 4.1.

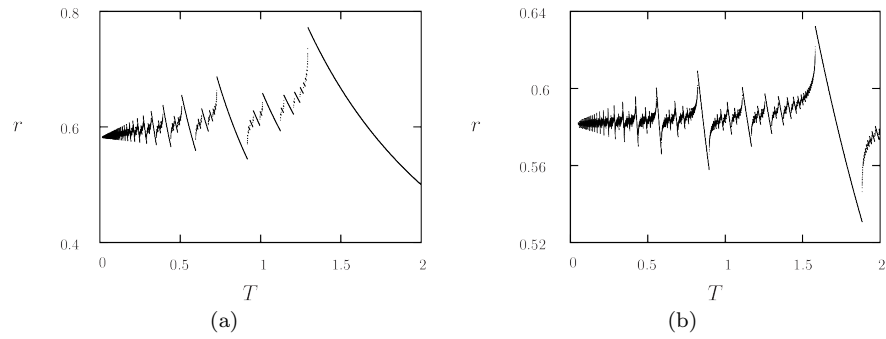


Figure 4.4: Magnification of figures 4.3 (b) and (d).



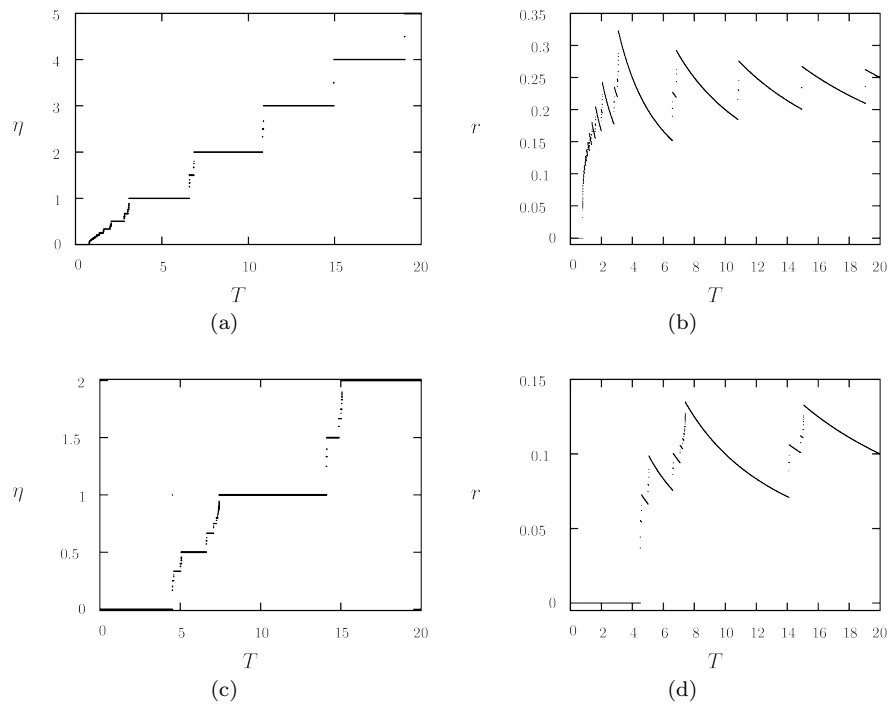


Figure 4.5: Same as Fig. 4.3 for  $Q = 0.257$ . (a) and (b):  $d = 0.2$  and  $1/A = 0.777$ . (c) and (d):  $d = 0.8$   $1/A = 3.111$ . As in the previous case, a global maximum occurs at  $T = T_1^{\mathcal{R}}$ ; however, the global minimum is 0 for a whole range of small periods.

### 4.3 Fixed dose for fixed pulse duration (amplitude correction)

We now fix the duration of the pulse  $\Delta$  and perform the dose conservation by properly modifying its amplitude. This is done by varying the parameters  $d$  and  $A$  along straight lines in the parameter space  $d \times 1/A$  parametrized by  $T$ ,

$$\left(d, \frac{1}{A}\right) = \left(\frac{\Delta}{T}, \frac{\Delta}{QT}\right). \quad (4.3)$$

Note that, with this approach, it is not possible to analyze the properties of the output when  $T \rightarrow 0$ , since its minimal value is  $T = \Delta$ . Varying  $T$  from  $\Delta$  to  $\infty$ , one has to vary  $(d, 1/A)$  from  $(1, 1/Q)$  to  $(0, 0)$  along a straight line with slope  $1/Q$  in order to keep the released energy constant.

Regarding the behavior of  $r(T)$  when  $T \rightarrow \infty$ , we can use proposition 3.3. From (4.3) we get  $d = \Delta/T$  and  $A = QT/\Delta$ , which, when combined with (4.2) and proposition 3.3 gives us

$$\lim_{T \rightarrow \infty} r(T) = \frac{Q}{\theta},$$

independently of  $\Delta$ .

In figure 4.6 we show the evolution of the firing rates for an input with average greater than the critical dose,  $Q_c$ . Note that this leads to a broken devil's staircase, as it starts at  $T = \Delta$ . The behavior at  $T \rightarrow \infty$  is the expected one.

In figure 4.7 we show the same computation for a  $Q < Q_c$ . In this case, if  $T$  is close enough to  $\Delta$ , equation (4.3) provides points located in the non-spiking region for which  $r(T) = \eta(T) = 0$ . Although the points provided by (4.3) are never located in the permanent-spiking region, they are in the conditional-spiking region if  $T$  is large enough. Hence, one starts observing spikes at some point.

Note that, unlike when fixing the dose by width correction, one always gets non zero spikes per period and non-zero firing rates, at least for small enough frequencies. This is because, when following the straight lines (4.3) towards the origin one always enters the spiking regions.

## 5 Conclusions

In this paper we have considered a generic spiking model (integrate-and-fire-like system) with an attracting equilibrium point in the subthreshold regime forced by means of a pulsatile (square wave) periodic input. As shown in [GKC13] the system exhibits spiking dynamics organized in rich bifurcation structures in the parameter space formed by the amplitude and duty cycle of the forcing pulse. We have studied how these structures, and dynamical properties associated with them, vary when the period of the forcing is varied while keeping the injected

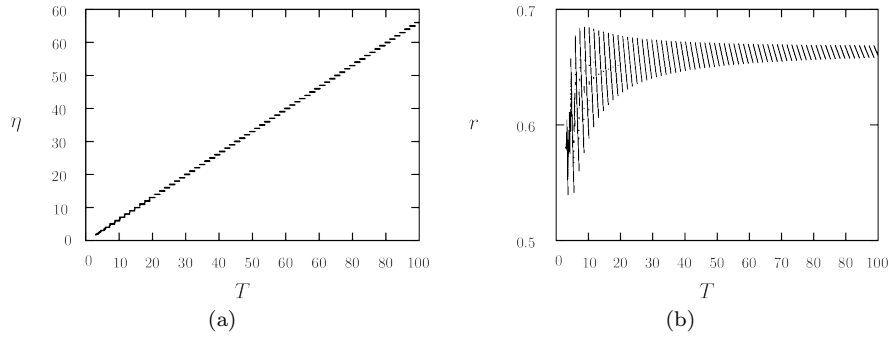


Figure 4.6: Firing-number (a) and firing rate (b) for  $Q = 0.666$  using amplitude correction while keeping constant the duration of the pulse,  $\Delta = 3$ .

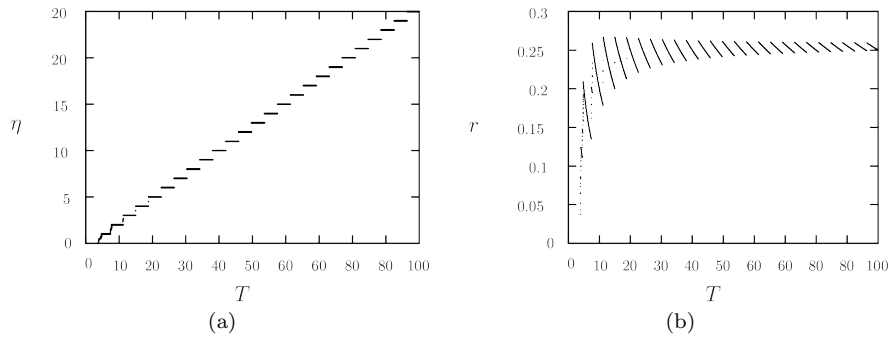


Figure 4.7: Firing-number (a) and firing rate (b) for  $Q = 0.257$  using amplitude correction while keeping constant the duration of the pulse,  $\Delta = 3$ .

dose (input average) constant. We have given special interest to the asymptotic firing rate (average number of spikes per unit time), which turns out to follow a devil's staircase (a fractal structure) with monotonically decreasing steps. In particular, we have precisely characterized its global maximum in the whole frequency domain as well each local maxima. If we consider specific ranges of frequency whose bounds correspond to the frequencies eliciting the subsequent local minima, the response can be decomposed in a repetitive structure with a non-monotonic, bell-shaped pattern and global maximum. In real life situations, the range of physically realistic frequencies is generally well delimited, as it is the case for the GnRH pulse frequency modulation responsible for the control of gonadotropin subunit expression. There exist other instances in endocrinology where gene expression is sensitive to the frequency of a pulsatile hormone. In the liver, a male pattern of cytochrome P450 expression is observed in response to low frequency GH (growth hormone) pulses, while a female pattern is induced by high frequency GH pulses [WPR<sup>+</sup>91].

When contrasted with real data, the mentioned characterization of the maxima of the system response for a generic system can be applied to design and calibrate simple models exhibiting the desired behaviour in a bounded frequency spectrum. Moreover, differences in the parameter values will lead to differences in the optimal frequency eliciting the maximal response, which can be at the source of a possible differential control by a single stimulus. In the case of the differential control exerted by GnRH frequency on the respective expression of FSH or LH  $\beta$  subunits, we can speculate that such differences could originate from different pathways in the GnRH signaling network and/or different values of some biochemical kinetic constants.

## References

- [BM61] N.N. Bogoliubov and Y.A. Mitropolski. *Asymptotic methods in the theory of non-linear oscillations*. Gordon and Breach, 1961.
- [BNXR10] S.P. Bliss, A.M. Navratil, J. Xie, and M.S. Roberson. GnRH signaling, the gonadotrope and endocrine control of fertility. *Front. Neuroendocrinol.*, 31:340–2010, 2010.
- [CB99] S. Coombes and P.C. Bressloff. Mode locking and arnold tongues in integrate-and-fire neural oscillators. *Phys. Rev E.*, 60:2086–2096, 1999.
- [CF07] F. Clément and J.-P. Françoise. Mathematical modeling of the GnRH pulse and surge generator. *SIAM J. Appl. Dyn. Syst. (SIADS)*, 6:441–456, 2007.
- [CO00] S. Coombes and A. H. Osbaldestin. Period-adding bifurcations and chaos in a periodically stimulated excitable neural relaxation oscillator. *Phys. Rev. E*, 62:4057–4066, 2000.

- [Coo01] S. Coombes. Phase-locking in networks of pulse-coupled mckean relaxation oscillators. *Physica D*, 2820:1–16, 2001.
- [COS01] S. Coombes, M. Owen, and G.D. Smith. Mode locking in a periodically forced integrate-and-fire-or-burst neuron model. *Phys. Rev E.*, 64:041914, 2001.
- [CTW12] S. Coombes, R. Thul, and K.C.A Wedgwood. Nonsmooth dynamics in spiking neuron models. *Physica D*, 241:2042–2057, 2012.
- [DHO+89] A.C. Dalkin, D.J. Haisenleder, G.A. Ortolano, T.R. Ellis, and J.C. Marshall. The frequency of gonadotropin-releasing-hormone stimulation differentially regulates gonadotropin subunit messenger ribonucleic acid expression. *Endocrinology*, 125:917–924, 1989.
- [EDGK97] N. Evans, G.E. Dahl, B.H. Glover, and F.J. Karsch. Central regulation of pulsatile gonadotropin-releasing hormone (GnRH) secretion by estradiol during the period leading up to the preovulatory GnRH surge in the ewe. *Endocrinology*, 138:1224–1231, 1997.
- [FG11] J.G. Freire and J.A.C. Gallas. Stern-brocot trees in cascades of mixed-mode oscillations and canards in the extended bonhoeffer-van der pol and the fitzhugh-nagumo models of excitable systems. *Phys. Lett. A*, 375:1097–1103, 2011.
- [GGT84] J.M. Gambaudo, P. Glendinning, and C. Tresser. Collage de cycles et suites de Farey. *C. R. Acad. Sc. Paris, série I*, 299:711–714, 1984.
- [GIT84] J.M. Gambaudo, O.Lanford III, and C. Tresser. Dynamique symbolique des rotations. *C. R. Acad. Sc. Paris, série I*, 299:823–826, 1984.
- [GKC13] A. Granados, M. Krupa, and F. Clément. Border collision bifurcations of stroboscopic maps in periodically driven spiking models. Preprint available at <http://arxiv.org/abs/1310.1054>, 2013.
- [KHR81] J.P. Keener, F.C Hoppensteadt, and J. Rinzel. Integrate-and-fire models of nerve membrane response to oscillatory input. *SIAM J. Appl. Dyn. Syst. (SIADS)*, 41:503–517, 1981.
- [KJSC97] U.B. Kaiser, A. Jakubowiak, A. Steinberger, and W.W. Chin. Differential effects of gonadotropin-releasing hormone (GnRH) pulse frequency on gonadotropin subunit and GnRH receptor messenger ribonucleic acid levels in vitro. *Endocrinology*, 138:1224–1231, 1997.
- [LC05] C.R. Laing and S. Coombes. Mode locking in a periodically forced “ghostbursting” neuron model. *Int. J. Bif. Chaos*, 15:1433, 2005.
- [MHR12] X. Meng, G. Huguet, and J. Rinzel. Type III excitability, slope sensitivity and coincidence detection. *Disc. Cont. Dyn. Syst.*, 32:2720–2757, 2012.

- [MK92] S.M. Moenter R.M. Brand A.R. Midgley and F.J. Karsch. Dynamics of gonadotropin-releasing hormone release during a pulse. *Endocrinology*, 130:503–10, 1992.
- [TB08] J. Touboul and R. Brette. Dynamics and bifurcations of the adaptive exponential integrate-and-fire model. *Biol. Cybernet*, 99:319–334, 2008.
- [TB09] J. Touboul and R. Brette. Spiking dynamics of bidimensional integrate-and-fire neurons. *SIAM J. Appl. Dyn. Syst. (SIADS)*, 4:1462–1506, 2009.
- [TBH<sup>+</sup>96] A.P. Thomas, G.S. Bird, G. Hajnczky, L.D. Robb-Gaspers, and J.W. Putney. Spatial and temporal aspects of cellular calcium signaling. *FASEB J.*, 10:1505–1517, 1996.
- [WPR<sup>+</sup>91] D.J. Waxman, N.A. Pampori, P.A. Ram, A.K. Agrawal, and B.H. Shapiro. Interpulse interval in circulating growth hormone patterns regulates sexually dimorphic expression of hepatic cytochrome p450. *Proc. Natl. Acad. Sci. USA*, 88(15):6868–6872, 1991.